Chemical Science

ROYAL SOCIETY OF CHEMISTRY

EDGE ARTICLE

View Article Online
View Journal | View Issue

Cite this: *Chem. Sci.*, 2022, **13**, 704

All publication charges for this article have been paid for by the Royal Society of Chemistry

Received 2nd September 2021
Accepted 14th December 2021

DOI: 10.1039/d1sc04855d

rsc.li/chemical-science

Stereoelectronic and dynamical effects dictate nitrogen inversion during valence isomerism in benzene imine†

Nilangshu Mandal, Ankita Das, Chandralekha Hajra and Ayan Datta *

Benzene imine (**1**) ⇌ 1*H*-azepine (**2**) isomerization occurs through sequential valence and *endo*–*exo* isomerism. Quantum chemical and quasiclassical trajectory (QCT) simulations reveal the coupled reaction pathway – ring-expansion followed by N-inversion to the most stable isomer, *exo*-1*H*-azepine (**Exo-2**). Direct-dynamics produce a mixture of *endo*- and *exo*-1*H*-azepine stereoisomers and govern the *endo*-1*H*-azepine (**Endo-2**) ⇌ *exo*-1*H*-azepine (**Exo-2**) ratio. **Exo-2** is computationally identified as the most stable product while **Endo-2** is fleetingly stable with a survival time (S_T) ~50 fs. *N*-Methyl substitution exclusively results in an *exo*-1-methyl-1*H*-azepine isomer. F-substitution at the N-site increases the barrier for N-inversion and alters the preference by stabilizing **Endo-2**. Interestingly, the *exo*-1-fluoro-1*H*-azepine (minor product) is formed through bifurcation *via* non-statistical dynamics. A highly concaved Arrhenius plot for **1a** → **2a** highlights the influence of heavy-atom tunneling on valence isomerism, particularly at low temperatures. Heavy-atom tunneling also results in a normal N–H(D) secondary KIE above 100 K even though the increase in hybridization from sp^2 to sp^3 at nitrogen should cause an inverse KIE classically.

Introduction

The equilibrium between bicyclo[4.1.0]hepta-2,4-diene and cyclo-hepta-1,3,5-triene has been a subject of active interest.[1] Ring-expansion is also known for oxygen (benzene-oxide ⇌ oxepin), nitrogen (benzene imine ⇌ 1*H*-azepine), sulfur (benzene sulfide ⇌ thiepine), and phosphorus (benzene phosphane ⇌ 1*H*-phosphepine).[2,3] All of them undergo disrotatory electrocyclic rearrangement to form the ring-opened product.[4] However, stereoelectronic induction can influence the reaction mechanism and conformations of strained molecules (see Scheme 1a).[5,6]

For example, 1*H*-azepine with 8π-electrons exists in a boat conformation as expected from its anti-aromatic Hückel electron count.[7] Based on DFT calculations, Dardonville *et al.* estimated an anti-aromatic destabilization of 10.8 kcal mol^{-1} for 1*H*-azepine by computing its protonation energies.[8] Ragyanszki and co-workers studied the oxidation of the anti-aromatic *N*-methyl-1*H*-azepine to the non-aromatic *N*-oxide of azepine.[9] 1*H*-Azepine, and its derivatives are also known to undergo rapid dimerization *via* (6 + 4)π *exo*-cycloaddition.[10]

Further, ring expansion of benzene imine into 1*H*-azepine (**1** → **2**) can in-principle also be accompanied by an inversion at the N-center (see Scheme 1b). Since the NMR spectra of 1*H*-

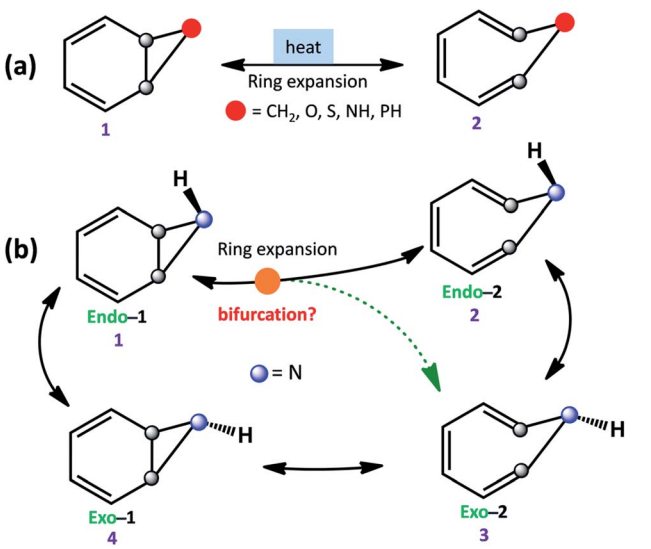

Scheme 1 (a) Ring expansion reactions in substituted bicyclo[4.1.0] hepta-2,4-dienes. (b) Schematic possible reaction pathways for benzene imine (**1**).

School of Chemical Sciences, Indian Association for the Cultivation of Science, 2A and 2B Raja S. C. Mullick Road, Jadavpur, Kolkata, 700032, West Bengal, India. E-mail: spad@iacs.res.in; Tel: +91-33-24734971

† Electronic supplementary information (ESI) available: Schematic potential energy surfaces, QCT inputs, details of MD simulations, QMT inputs, CVT and CVT + SCT rates for valence isomerism, NBO analyses, Cartesian coordinates, energies, and harmonic frequencies and Awk Code. See DOI: 10.1039/d1sc04855d

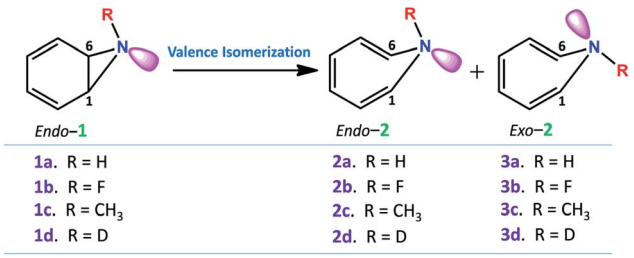

Scheme 2 Valence isomerism in benzene imine (**1**) derivatives to their 1H-azepine (**2**) analogs.

azepine remain invariant in the range −90 °C to + 130 °C, Paquette *et al.* suggested that the inversion barrier should be less than 5.7 kcal mol^{-1}.[11] Additionally, they could not gather any signature for the existence of benzene imine in this temperature range. Therefore, **Exo-2** is expected to be the thermodynamically most stable product. However, the mechanism is still unknown and a possible reaction pathway can be either stepwise (**1** → **2** → **3**) or coupled (**1** → **2**, **3**) for the formation of 1*H*-azepine analogs.

In Scheme 2, we have used different substitutions at the N-site to examine the stereoelectronic effects on the valence isomerization of **Endo-1**. Obtaining a detailed reaction mechanism and understanding the effect of the stereoelectronic influence on the potential energy surface for the **Endo-1** → **Endo-2**/**Exo-2** isomerizations require further time-resolved mechanistic investigation using quasi-classical MD simulations.[12–14] Additionally, the dynamics at sub-cryogenic temperatures would be dictated by quantum mechanical tunneling (QMT) instead of over-the-barrier crossing at ambient temperatures.[15–27] In this context recently, Sander and co-workers have reported unequivocal signatures of heavy-atom tunneling for the benzene oxide – oxepin equilibrium at 3 K.[28] The present article investigates post-transition state bifurcation reaction pathways for benzene imine ⇌ 1*H*-azepine. MD simulations were performed from the rate-limiting transition states to decipher the non-statistical effects on the stereoselectivity (**Endo-2** : **Exo-2**) during the valence isomerism.[29] Heavy-atom tunneling is shown to be the major pathway for ring expansion, particularly at low temperatures.

Computational details

Geometry optimization was performed at the M06-2X/6-31+G(d,p) level of theory with the Gaussian 16 (ver A.03) suite of programs (see the ESI, Page S2† for calibration and benchmarking).[30,31] Reaction energies and activation barriers were investigated for **Endo-1** → **Exo-1**, **Endo-2**, **Exo-2**, and their analogs (R = –F, and $–CH_3$). The reactant, product, and transition-state were confirmed by intrinsic reaction coordinate (IRC) and harmonic frequency calculations.[32] In addition, for computation of the reaction rates at low temperatures, the transition states (TS) were located using canonical variational transition-state theory (CVT) along the reaction path *s* where free-energy maximizes at the same level as used for geometry minimization.[33] Tunneling corrections were incorporated within the rate coefficient calculations using the small-curvature tunneling (SCT) approximation.[34] These were implemented within Gaussrate 17-B by interfacing with Gaussian 16 and Polyrate 17-C.[35,36] Quantized reactant state tunneling (QRST) calculations were performed to determine the reaction rates accurately at sub-cryogenic temperatures.[37]

Further, the ambient temperature behavior of **Endo-1** for R = –H, –F, and $–CH_3$ was studied using quasiclassical direct-dynamics simulations in the gas phase at 298.15 K. Reaction trajectories were simulated from rate-limiting sampled **TS(1** → **2)** structures using the Singleton's Progdyn code interfaced with Gaussian 16 (see the ESI for TS-sampling details, Fig. S4†).[38–41] The reaction trajectories were simulated to the forward and backward directions until either one of the products or the reactants is formed. The classical equations of motion were integrated with a velocity-Verlet algorithm.[42] The energies and derivatives were calculated on the fly with the M06-2X/6-31+G(d,p) level. The time step for integration is 1 fs. Thresholds for bond formations, trajectory terminations, and in-house code for trajectory characterization are shown on Page S8 and S50.†

Results and discussion

Benzene imine (**Endo-1**) can isomerize to *exo*-1*H*-azepine (**Exo-2**) either by ring expansion followed by N-inversion or *vice versa*. Both the plausible pathways are presented in Fig. 1.

Each involves two steps and crossing two barriers, namely **1** → **2** → **3** or **1** → **4** → **3** with $\Delta G^{\ddagger}_{1\rightarrow 2}$ followed by $\Delta G^{\ddagger}_{2\rightarrow 3}$ or $\Delta G^{\ddagger}_{1\rightarrow 4}$ followed by $\Delta G^{\ddagger}_{4\rightarrow 3}$ respectively. The kinetic preference

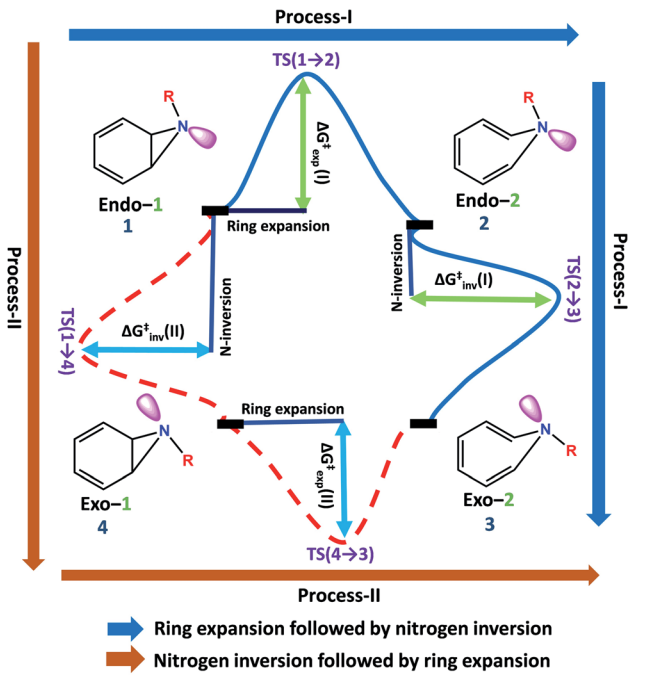

Fig. 1 Two plausible mechanistic pathways for the formation of *exo*-1*H*-azepine, **Exo-2** from benzene imine, **Endo-1**.

Table 1 Relative free energies and free energies of activation at 298.15 K (in kcal mol^{-1}) for **1** → **2** → **3** and **1** → **4** → **3** at the M06-2X/6-31+G(d,p) level of theory

	1a (R = H)	**1b** (R = F)	**1c** (R = CH_3)
1 (**Endo-1**)	0.0	0.0	0.0
$\Delta G^{\ddagger}_{1\to2}$	4.4	5.7	5.2
2 (**Endo-2**)	0.3	−0.1	0.6
$\Delta G^{\ddagger}_{2\to3}$	1.4	6.7	0.5
3 (**Exo-2**)	−2.7	−2.0	−3.8
$\Delta G^{\ddagger}_{1\to4}$	18.0	—	17.1
4 (**Exo-1**)	3.7	−0.5	1.4
$\Delta G^{\ddagger}_{4\to3}$	5.5	6.4	4.3

of either depends on the relative magnitudes of these barriers. Table 1 lists them for the various substituents on the nitrogen head. The *exo*-1*H*-azepine **Exo-2** is the most stable isomer irrespective of the substituent. Therefore, the benzene imine ⇌ 1*H*-azepine equilibrium will shift towards the 1*H*-azepine side. This result is in agreement with previous experiments.[11]

In terms of the preference for either **1** → **2** → **3** or **1** → **4** → **3** (see Fig. 1), ring expansion followed by the inversion pathway (a process-I) is more favorable than inversion followed by expansion (process-II). For example, in **1a**, $\Delta G^{\ddagger}_{1\to2}$ = 4.4 kcal mol^{-1} and $\Delta G^{\ddagger}_{2\to3}$ = 1.4 kcal mol^{-1} while $\Delta G^{\ddagger}_{1\to4}$ = 18.0 kcal mol^{-1} and $\Delta G^{\ddagger}_{4\to3}$ = 5.5 kcal mol^{-1}.

The high inversion barrier for **Endo-1** → **Exo-1** ($\Delta G^{\ddagger}_{1\to4}$ (inversion) = 18.0 and 17.1 kcal mol^{-1} for **1a** and **1c** respectively) arises due to the ring-strain in the three-membered aza-ring, which aggravates in the transition-state due to the planarity of the N-site. In contrast, the stereoelectronic modulation using R = –F leads to the cleavage of the bridging bond (rate-limiting step) of the **1b** and disfavors the planarity of N–F with the cyclopropane ring in **TS**(**1** → **4**) for the **1** → **4** → **3** reaction pathway and therefore, its TS could not be located (process-II).[43]

Following the kinetically favorable **1** → **2** → **3** pathway (coupled valence isomerism along the C–C bond and *endo–exo* isomerism *via* N-inversion) **1a**, **1b**, and **1c** show remarkable variation in their relative $\Delta G^{\ddagger}_{1\to2}$ (expansion) and $\Delta G^{\ddagger}_{2\to3}$ (inversion). For **1a** the free-energy of activation for ring expansion is three times more than that for inversion, while for **1b**, both the barriers are comparable. For **1c**, the activation barrier for N-inversion is the smallest, $\Delta G^{\ddagger}_{2c\to3c}$ = 0.5 kcal mol^{-1}. Ironically, **1b** and **1c** are isoelectronic, yet their significant differences in the N-inversion barriers make them ideal candidates to compare the product distributions between *endo*- and *exo*-1*H*-azepine conformational isomers *viz.* **2b**/**3b** and **2c**/**3c** and contrast with the parent benzene imine ⇌ 1*H*-azepine, **2a**/**3a**. See ESI Fig. S1–S3† for schematic potential energy surfaces for **1a**, **1b**, and **1c**.

Valence isomerism in *endo*-benzene imine is an example of a dynamically rich system where rapid C–C bond dissociation assists N–H inversion. The rate-limiting C1–C6 bond activation facilitates both the ring expansion and N-inversion (see Fig. 2). The quasiclassical direct-MD simulations reveal a chameleonic transition state **TS**(**1a** → **2a**) and the non-statistical effects on the product count (**Endo-2** : **Exo-2**).[44–48]

Fig. 2 depicts a typical trajectory and the time-resolved formation of azepine isomers (**2a** and **3a**). A total of 142 reaction trajectories were propagated from rate-limiting **TS**(**1a** → **2a**) (see ESI Fig. S4† for details). The reaction trajectories passing through the **TS**(**1a** → **2a**) zone can be characterized as "normal" trajectories if they follow the IRC-pathway (**1** → **2** → **3**) or "flyby" trajectories when they skip the minimum energy pathway (bypassing the **2a**-zone) and directly traverse to **TS**(**2a** → **3a**), finally forming **3a**.

Out of the 142 reaction trajectories, 108 (76%) "normal" reaction trajectories led to *exo*-1*H*-azepine (**3a**) while 20 (14%) "flyby" reaction trajectories afford the **TS**(**2a** → **3a**) and finally fall to the *exo*-1*H*-azepine (**3a**) zone. Only 6 (4%) trajectories are

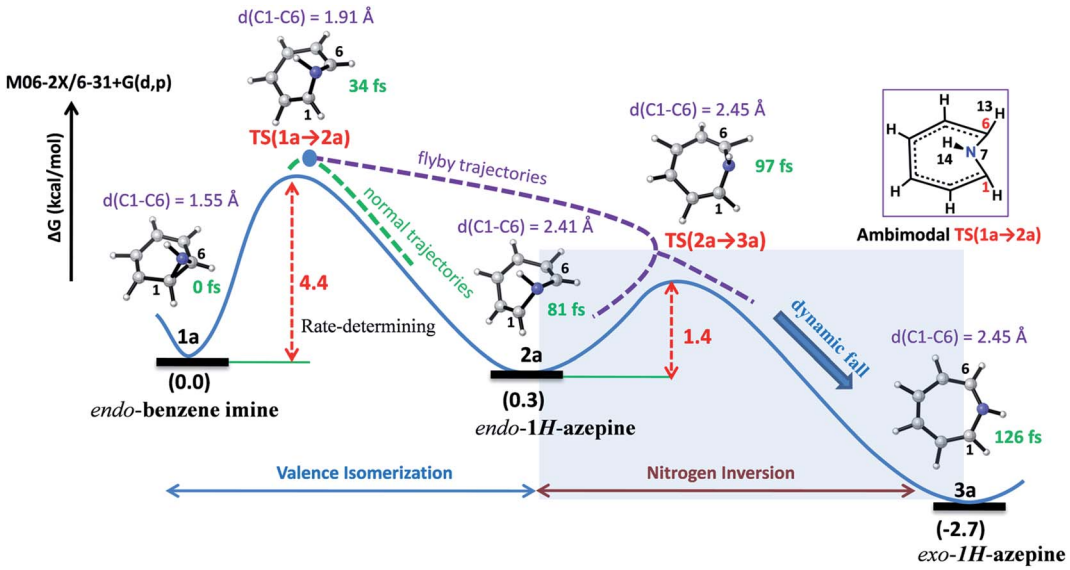

Fig. 2 Representative reaction pathways for the valence isomerization assisted nitrogen inversion of **1a**.

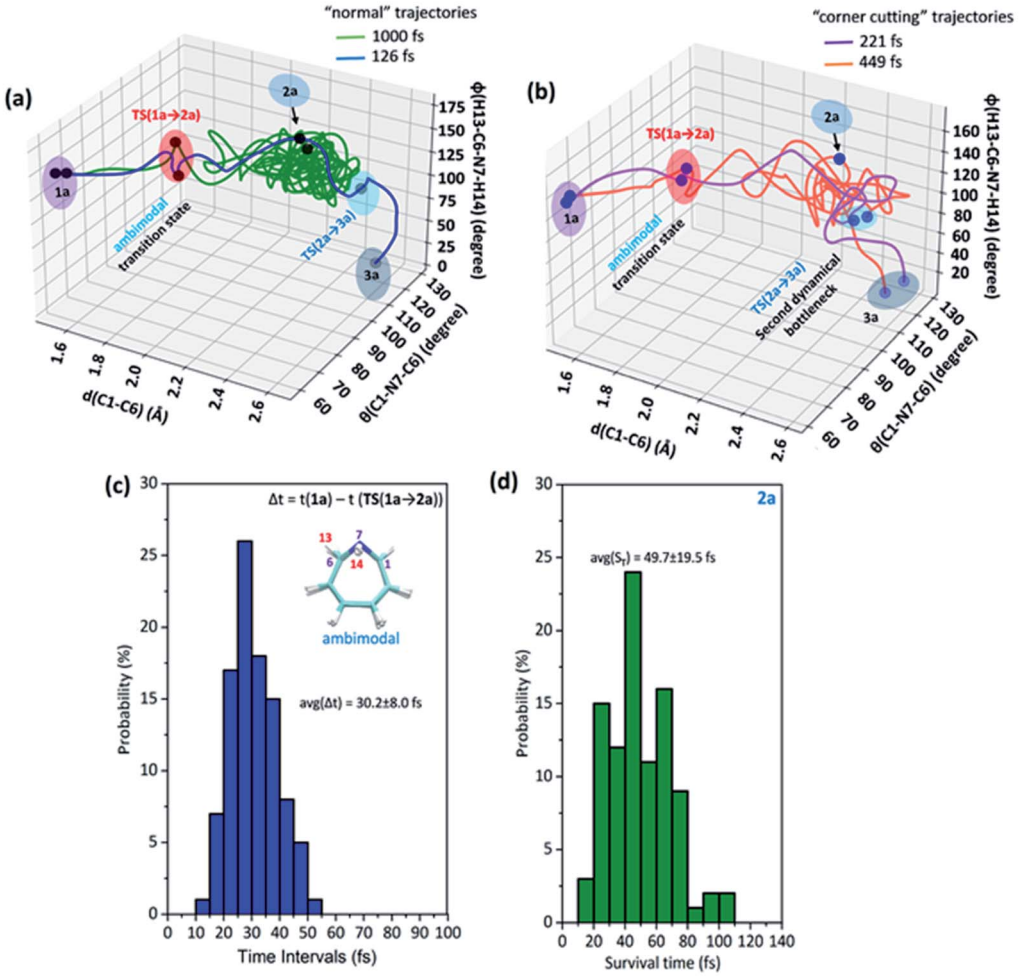

Fig. 3 (a) "Normal" trajectories represent the pathways for the formation of **2a** and **3a**, (b) "flyby" trajectories traverse to TS(**2a** → **3a**) and eventually fall to the **3a** product side, the (c) average time (Δt) required for the **1a** → TS(**1a** → **2a**) path and the (d) average survival time (S_T) for the endo-1*H*-azepine (**2a**) product.

found in the simulation that produces *endo*-1*H*-azepine (**2a**) up to 1 ps. The remaining 8 (6%) re-cross to either the reactant (**1a**) or product (**3a**) zones. This indicates a post-transition state bifurcation reaction where dynamical effects govern the stereoselectivity. The selectivity (**2a** : **3a**) for the **1a** → **2a**, **3a** ring-opening reaction is ~1 : 21.

Further, Fig. 3(a) represents two "normal" reaction trajectory propagations and time-resolved variation of the critical structural parameters (d, θ, and ϕ) during valence isomerization (benzene imine → 1*H*-azepine). The green-colored trajectory defines the reaction path that affords *endo*-1*H*-azepine (**2a**) which is found stable up to 1 ps during MD simulation. In contrast, the blue trajectory follows the ultrafast decay along the steepest descent path and eventually falls towards the *exo*-1*H*-azepine (**3a**) product zone.

These flyby reaction trajectories were found highly concerted and follow shorter dynamical routes to reach the **3a**-product zone in the potential energy surface. In Fig. 3(b) a typical "flyby" trajectory (violet line) shows its transit from **TS**(**1a** → **2a**) to **TS**(**2a** → **3a**) and falls into the **3a**-product basin without forming **Endo-2** (**2a**). On the other hand, the orange line first approaches the **TS**(**2a** → **3a**) zone, takes a short trip at the **2a**-zone, and finally populates the *exo*-1*H*-azepine, **Exo-2** (**3a**) basin.[49]

Further, the lower thermodynamic stability of *endo*-1*H*-azepine (ΔG (**2a** and **3a**) = 3.0 kcal mol^{-1}) and small activation barrier ($\Delta G^{\ddagger}$ = 1.4 kcal mol^{-1}) for the N–H inversion populates the **3a** product basin. From Fig. 3(c), we can estimate that the average time (Δt) required to reach the rate-limiting transition state **TS**(**1a** → **2a**) is 30.2 ± 8.0 fs. We have also calculated the survival time (S_T) using the cut-offs: **2a** appears when d(C1–C6) > 2.19 Å, θ(C1–N7–C6) > 98° and ϕ(H13–C6–N7–H14) > 135° whereas **2a** disappears when d(C1–C6) > 2.38 Å, θ(C1–N7–C6) > 98° and ϕ(H13–C6–N7–H14) > 104°. The survival time (S_T) *vs.* probability plot indicates that the average survival time (S_T) of **2a** is 49.7 ± 19.5 fs (see Fig. 3(d)). Therefore, the signature of the *endo*-1*H*-azepine (**2a**) formation can be traced using spectroscopic techniques.[50,51]

Additionally, the electronic and dynamical effect control on stereoselectivity was investigated by introducing R = –F and

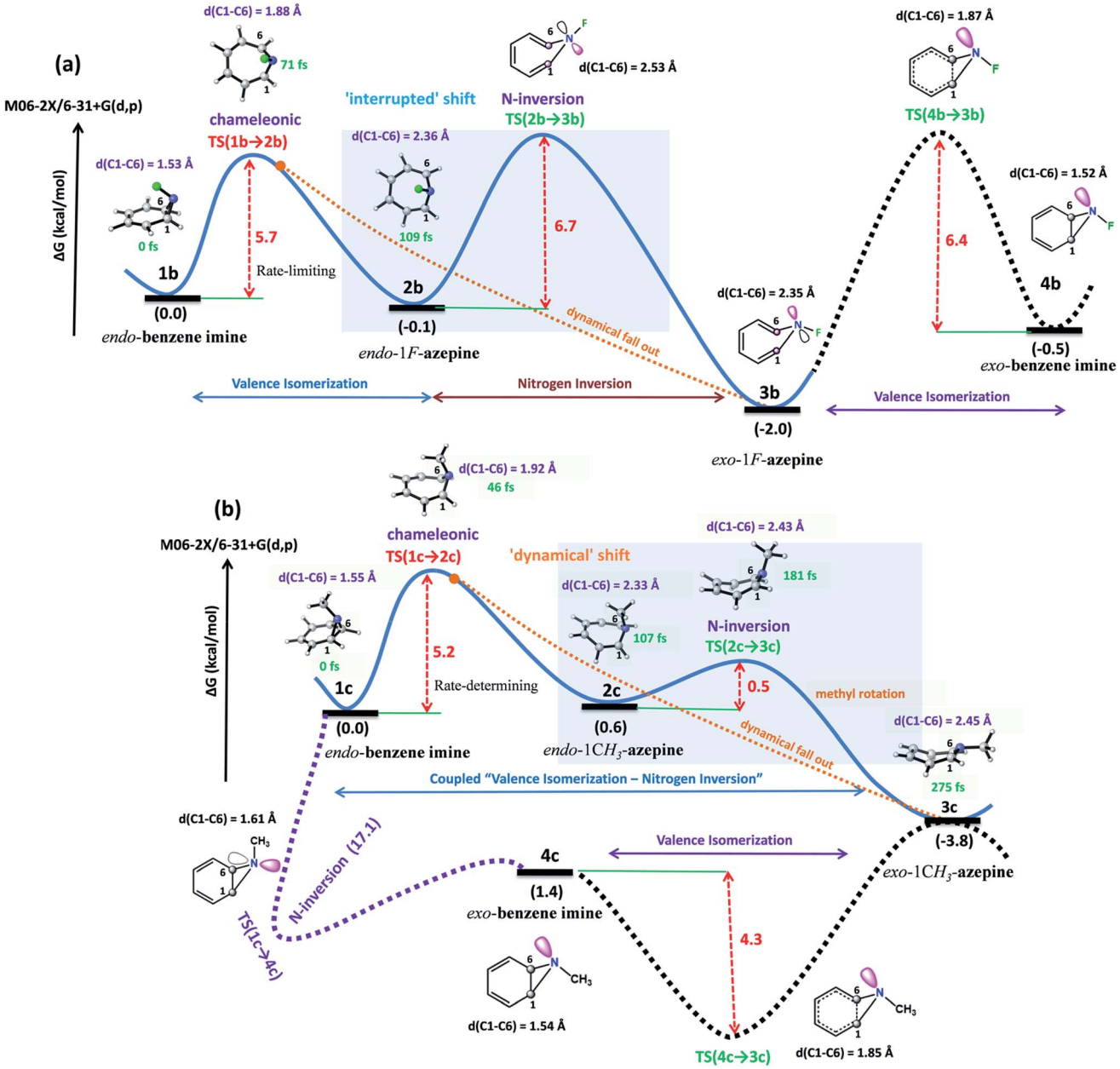

Fig. 4 (a and b) Evolution of the potential energy surfaces, where "interrupted" shift and "dynamical" shift denote the modification strategies to isolate the *endo*-1*F*-azepine (**2b**) and *exo*-1CH_3-azepine (**3c**), respectively.

–CH_3 at the inversion center. In Fig. 4(a), the relative free energy surface dictates an "interrupted" shift.[52] The valence isomerism mediated inversion is decoupled at *endo*-1*F*-azepine (**2b**). In general, we can apply such a potential energy surface manipulation strategy either by stabilizing **Endo-2** or destabilizing the N-inversion barrier for these coupled reactions. Interestingly, the stronger electron-withdrawing substitutions not only increase the **Endo-2** → **Exo-2** inversion barrier but also disfavors the transition state of direct **Endo-1** → **Exo-1** isomerization. In the case of –F substitution, the **1b** → **2b** → **3b** → **4b** pathway connects **1b** ⇄ **4b**. In contrast, **TS**(**1c** → **4c**) connects **1c** ⇄ **4c** (**Endo-1** → **Exo-1**) with a significantly higher activation energy barrier (E_a = 17.1 kcal mol^{-1}). However, such isolobal –CH_3 stereoelectronic induction accelerates the formation of *exo*-1CH_3-azepine (**3c**) (see, Fig. 4(b)). In this case, **2c** → **3c** isomerization has such a small barrier which makes it a highly coupled pathway (**1c** → **3c**), a "dynamical" shift.[48]

In Fig. 4(a) and (b), snapshots of typical trajectories are shown. The reaction trajectories are simulated from these rate-limiting transition states, **TS**(**1b** → **2b**) and **TS**(**1c** → **2c**) respectively. In the case of –F substitution, a typical trajectory affords **2b** (**Endo-2**) within 109 fs and is stable in the simulation. However, the representative reaction trajectory forms **3c** (**Exo-2**) within 275 fs.

The 3D plots depict the typical trajectories simulated from rate-limiting TSs, **TS**(**1b** → **2b**) and **TS**(**1c** → **2c**) respectively

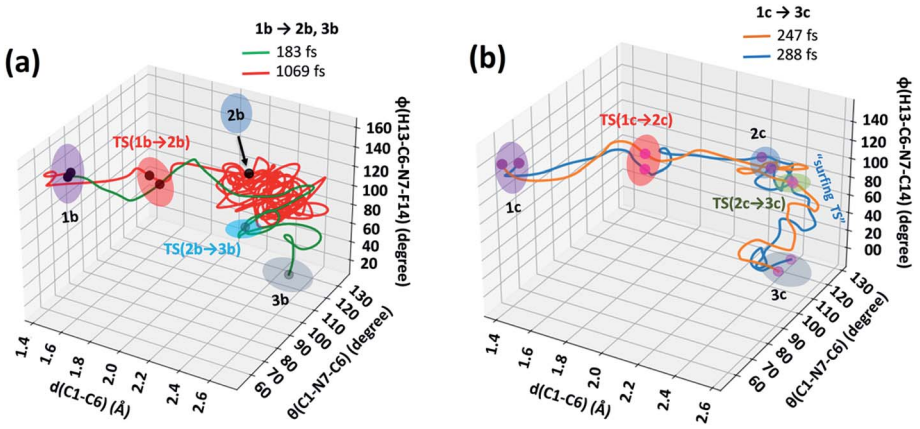

Fig. 5 3D-reaction plots for the valence isomerism reactions of (a) **1b** → **2b**, **3b** and (b) **1c** → **3c**.

(see Fig. 5). In Fig. 5(a), two typical reaction trajectories are depicted. The red "normal" reaction trajectory elucidates the formation of **2b** *via* the steepest descent path (IRC-pathway), whereas the green flyby route shows the dynamical pathway (non-statistical) that can afford *exo*-product **3b** formation for the valence isomerism in **1b**. On the other hand, the orange and blue lines show fast conversion into the *N*-methyl substituted *exo*-1*H*-azepine (**3c**) (see Fig. 5(b)).

Further, we performed 156 reaction trajectorie simulations from the **TS**(**1b** → **2b**) at the M06-2X/6-31+G(d,p) level of theory (see ESI Fig. S4 and S5† for details). In this case, out of 132 (85%) product forming reaction trajectories, 87 (56%) afford *endo*-1*F*-azepine, **2b**. Interestingly, 45 (29%) reaction trajectories follow the dynamical (non-statistical pathways) routes to reach the *exo*-product (**3b**) zone. Therefore, the R = –F stereoelectronic modulation manipulates the stereoselectivity of the valence isomerism in **1b**. The stereoselectivity (**2b** : **3b**) of the reaction is 2 : 1.

In addition, a total of 145 reaction trajectories are propagated from the **TS**(**1c** → **2c**) at the same level of theory (see ESI Fig. S4 and S5† for details). Out of 141 (97%) productive trajectories, 104 (72%) follow the IRC path. Interestingly, out of 37 (25%) "corner cutting" reaction trajectories, 36 directly traverse through the N–CH_3 inversion **TS**(**2c** → **3c**) and further dynamically fall out to the **3c**-zone, whereas only 1 "flyby" reaction trajectory leads to **2c**-product *via* **TS**(**2c** → **3c**). We found that *exo*-1-methyl-1*H*-azepine **3c** was the exclusive product (**Endo-2** : **Exo-2**= 1 : 140).

On the other hand, out of 104 "normal" reaction trajectories, 32 were dynamically stepwise. The 32 stepwise trajectories "surf" the **TS**(**2c** → **3c**) dividing the surface before leaving the TS zone. The average surfing time at the **TS**(**2c** → **3c**) zone is 20.2 ± 7.4 fs (see the ESI, Fig. S5†). This is due to the conformational penalty which the methyl group needs to incur along the path **1c** → **TS**(**2c** → **3c**) while passing through the **TS**(**2c** → **3c**) dividing the potential landscape. Quasielastic neutron scattering experiments are well-suited to recognize methyl-rotations in dynamically rich systems.[53]

Further, quantum mechanical tunneling (QMT) effects are investigated and they significantly dictate the benzene imine ⇌

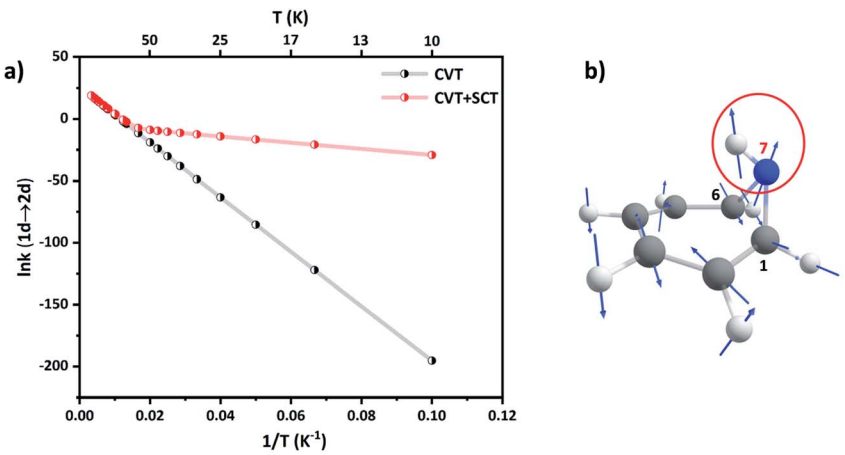

Fig. 6 (a) Arrhenius plot of the CVT and CVT + SCT rates (in s^{-1}) for **1a** → **2a**. (b) Displacement vectors for the normal mode of **TS**(**1a** → **2a**). The directional motion of the N7–H bond is encircled.

1*H*-azepine dynamics. Considering that $\Delta G^{\ddagger}_{\mathbf{1}\rightarrow\mathbf{2}}$ (expansion) is the rate-limiting step along the preferred **1** → **2** → **3** pathway, ring isomerization of *endo*-benzene imine (**Endo-1**) to *endo*-1*H*-azepine (**Endo-2**) essentially would involve motion of the two bridged carbons (C1 and C6 in Scheme 2). A qualitative estimation of the width of the barrier (w) is obtained by the difference in d(C1–C6) between the benzene imine and azepine. For **1a** → **2a**, w is only 0.75 Å which along with a small $\Delta G^{\ddagger}_{\mathbf{1a}\rightarrow\mathbf{2a}}$ = 4.4 kcal mol^{-1} makes a strong case for heavy-atom tunneling.[54,55]

Since ring expansion is endergonic along **1a** → **2a**, the reaction rates are obtained by performing SCT dynamical calculations along the reverse (exergonic) direction followed by scaling them by microscopic reversibility.[56] At 300 K, $k^{\mathrm{CVT+SCT}}$ (**1a** → **2a**) = 1.84 × 10^{8} s^{-1} while k^{CVT} (**1a** → **2a**) = 1.75 × 10^{8} s^{-1}, acceleration by only 5% due to tunneling. However, at the liquid N_2 temperature, $k^{\mathrm{CVT+SCT}}$ (**1a** → **2a**) and k^{CVT} (**1a** → **2a**) are 1.51 × 10^{-1} s^{-1} and 3.64 × 10^{-2} s^{-1}, respectively, a gain of 75% by tunneling. The Arrhenius plot of the reaction rate shows strong curvature at low temperatures in Fig. 6(a). At 40 K, $k^{\mathrm{CVT+SCT}}$ (**1a** → **2a**) = 3.12 × 10^{-5} s^{-1} which is nine-orders more than the pure classical over-the-barrier transit. Such large enhancements in reaction rates at sub-cryogenic temperatures make ring-opening a highly QMT driven process.

Ring expansion along the C1–C6 bond also remotely affects the N–H bond at the bridgehead. The C1–N7–C6 bond angle increases from θ(C1–N7–C6) = 63.9° in **1a** to θ(C1–N7–C6) = 82.4° in **TS**(**1a** → **2a**). Natural Bond Orbital (NBO)[57] calculations at the M06-2X/6-31+G(d,p) level (see the ESI, Table ST5†) show that the hybridization at the N-center changes from sp^2 to sp^3. This should classically result in an inverse secondary KIE.[58] Indeed, secondary H/D isotope effects at CVT are inverse at all temperatures. For example, k^{CVT} (**1a** → **2a**)/k^{CVT} (**1d** → **2d**) = 0.96, 0.89 and 0.32 at T = 300 K, 100 K and 10 K respectively. However, the normal mode for ring-expansion also shows motion along the N–H(D) bond in the translation vector for the TS, see Fig. 6(b). Therefore, because the H-atom is lighter than D, tunneling assists **1a** → **2a** preferentially over **1d** → **2d**. This makes the secondary KIE positive at high temperatures and reduces the extent of inverse secondary KIE with $k^{\mathrm{CVT+SCT}}$ (**1a** → **2a**)/$k^{\mathrm{CVT+SCT}}$ (**1d** → **2d**) = 1.08, 1.03, and 0.42 at T = 300 K, 100 K, and 10 K respectively.

Conclusion

Post-transition-state dynamics and quantum mechanical tunneling play an important role in the benzene imine ⇌ 1*H*-azepine equilibrium. This isomerism belongs to a peculiar class of pericyclic reactions where ring expansion dictates stereoselectivity. The C–C bond cleavage and N-inversion dynamics guide the rich diversity of *endo*-/*exo*-product outcomes. The dynamics can be selectively controlled by the electronic nature of the substituents on the N-end. While a strong electron-withdrawing group like –F decouples the ring-expansion and inversion pathways, for the –H/–CH_3 groups they are strongly entangled to result in the final ring-expanded form with N-inversion. At sub-cryogenic temperatures when the reaction is driven by quantum mechanical tunneling, heavy-atom tunneling governs the reaction due to the small width of the barrier for ring expansion. Such coupled valence isomerism and N-inversion are also anticipated for other norcaradienes wherein the stereoelectronic effects of the substituents are critical.

Data availability

The datasets supporting this article have been uploaded as part of the ESI.†

Author contributions

NM performed the research, Ankita ran QMT calculations; CH did dynamics setup; AD planned the project.

Conflicts of interest

The authors declare no competing financial interests.

Acknowledgements

NM thanks CSIR for SRF. AD and CH thank DST Inspire and IACS for the research fellowship. AD thanks TRC-DST and SERB grant no. DIA/2018/000013 and CRG/2020/000301 for partial funding.

References

1 T. L. Gilchrist and R. C. Storr, *Organic Reactions and Orbital Symmetry*, Cambridge University Press, Cambridge, 2nd edn, 1979.
2 E. Vogel and H. Gunther, Benzene Oxide – Oxepin Valence Tautomerism, *Angew. Chem., Int. Ed. Engl.*, 1967, **6**, 385–401.
3 L. A. Paquette, Valence Isomerism in Selected Heterocyclic Systems, *Angew. Chem., Int. Ed. Engl.*, 1971, **10**, 11–20.
4 H. Jansen, J. C. Slootweg and K. Lammertsma, Valence Isomerism of Cyclohepta-1,3,5-triene and its Heteroelement Analogues, *Beilstein J. Org. Chem.*, 2011, **7**, 1713–1721.
5 I. V. Alabugin, *Stereoelectronic Effects: A Bridge Between Structure and Reactivity*, John Wiley & Sons, Ltd, Chichester, UK, 2016.
6 D. H. Ess, S. E. Wheeler, R. G. Lafe, L. Xu, N. Çelebi-Ölçüm and K. N. Houk, Bifurcations on Potential Energy Surfaces of Organic Reactions, *Angew. Chem., Int. Ed.*, 2008, **47**, 7592–7601.
7 L. A. Paquette, D. E. Kuhla, J. H. Barrett and R. J. Haluska, Unsaturated Heterocyclic Systems. LII. A General Synthetic Entry to Derivates of 1H-Azepine, *J. Org. Chem.*, 1969, **34**, 2866–2878.
8 C. Dardonville, M. L. Jimeno, I. Alkorta and J. Elguero, Homoheteroaromaticity: The Case Study of Azepine and Dibenzazepine, *Org. Biomol. Chem.*, 2004, **2**, 1587–1591.
9 R. Fournier, A. R. Green, A. Greenberg, E. Lee-Ruff, J. F. Liebman and A. Ragyanszki, Predicted Reversal in N-

Methylazepine/N-Methyl-7-azanorcaradiene Equilibrium Upon Formation of their N-Oxides, *Molecules*, 2020, **25**, 4767.

10 L. A. Paquette, D. E. Kuhla and J. H. Barrett, Unsaturated Heterocyclic Systems. LIII. Thermochemical Reactions of 1H-Azepine Derivatives. II. Aromatization and Sigmatropic Migrations Involving Nitrogen, *J. Org. Chem.*, 1969, **34**, 2879–2884.

11 L. A. Paquette, J. H. Barrett and D. E. Kuhla, Thermochemical Reactions of 1H-Azepine Derivatives. I. Dimerization, *J. Am. Chem. Soc.*, 1969, **91**, 3616–3624.

12 K. Black, P. Liu, L. Xu, C. Doubleday and K. N. Houk, Dynamics, Transition States, and Timing pf Bond Formation in Diels–Alder Reactions, *Proc. Natl. Acad. Sci. U. S. A.*, 2012, **109**, 12860–12865.

13 J. Rehbein and B. K. Carpenter, Do we fully understand what controls chemical selectivity?, *Phys. Chem. Chem. Phys.*, 2011, **13**, 20906–20922.

14 J. M. Burns, Computational evidence for a reaction pathway bifurcation in Sasaki-type (4 + 3)-cycloadditions, *Org. Biomol. Chem.*, 2018, **16**, 1828–1836.

15 N. Mandal, A. K. Pal, P. Gain, A. Zohaib and A. Datta, Transition-State-like Planar Structures for Amine Inversion along Ultralong C–C Bonds in Diamino-*o*-carborane and Diamino-*o*-dodecahedron, *J. Am. Chem. Soc.*, 2020, **142**(11), 5331–5337.

16 C. Castro and W. L. Karney, Heavy-Atom Tunneling in Organic Reactions, *Angew. Chem., Int. Ed.*, 2020, **59**, 8355–8366.

17 S. K. Sarkar, E. Solel, S. Kozuch and M. Abe, Heavy-Atom Tunneling Processes during Denitrogenation of 2,3-Diazabicyclo[2.2.1]hept-2-ene and Ring Closure of Cyclopentane-1,3-diyl Diradical. Stereoselectivity in Tunneling and Matrix Effect, *J. Org. Chem.*, 2020, **85**(14), 8881–8892.

18 P. R. Schreiner, Quantum Mechanical Tunneling is Essential to Understand Chemical Reactivity, *Trends Chem.*, 2020, **2**, 980–989.

19 X. Zhang, D. A. Hrovat and W. T. Borden, Calculations Predict That Carbon Tunneling Allows the Degenerate Cope Rearrangement of Semibullvalene to Occur Rapidly at Cryogenic Temperatures, *Org. Lett.*, 2010, **12**, 2798–2801.

20 D. Gerbig, D. Ley and P. R. Schreiner, Light- and Heavy-Atom Tunneling in Rearrangement Reactions of Cyclopropylcarbenes, *Org. Lett.*, 2011, **13**(13), 3526–3529.

21 C. Doubleday, R. Armas, D. Walker, C. V. Cosgriff and E. M. Greer, Heavy-Atom Tunneling Calculations in Thirteen Organic Reactions: Tunneling Contributions are Substantial, and Bell's Formula Closely Approximates Multidimensional Tunneling at ≥250K, *Angew. Chem., Int. Ed.*, 2017, **129**, 13279–13282.

22 B. K. Carpenter, Heavy-atom tunneling as the dominant pathway in a solution-phase reaction? Bond shift in antiaromatic annulenes, *J. Am. Chem. Soc.*, 1983, **105**(6), 1700–1701.

23 M. Ertelt, D. A. Hrovat, W. T. Borden and W. Sander, Heavy-Atom Tunneling in the Ring Opening of a Strained Cyclopropene at Very Low Temperates, *Chem.–Eur. J.*, 2014, **20**(16), 4713–4720.

24 I. Sedgi and S. Kozuch, Heavy atom tunnelling on XeF_6 pseudorotation, *Phys. Chem. Chem. Phys.*, 2020, **22**, 17725–17730.

25 C. M. Nunes, I. R. Eckhardt, R. Fausto and P. R. Schreiner, Competitive Nitrogen versus Carbon Tunneling, *J. Am. Chem. Soc.*, 2019, **141**(36), 14340–14348.

26 C. M. Nunes, I. Reva, S. Kozuch, R. J. McMohan and R. Fausto, Photochemistry of 2-Formylphenylnitrene: A Doorway to Heavy-Atom Tunneling of a Benzazinine to a Cyclic Ketenimine, *J. Am. Chem. Soc.*, 2017, **139**(48), 17649–17659.

27 S. Karmakar and A. Datta, Heavy-atom tunneling in organic transformations, *J. Chem. Sci.*, 2020, **132**, 1–22.

28 T. Schleif, M. P. Merini and W. Sander, The Mystery of the Benzene-Oxide/Oxepin Equilibrium – Heavy-Atom Tunneling Reversed by Solvent Interactions, *Angew. Chem., Int. Ed.*, 2020, **59**, 20318–20322.

29 X. Ma and W. L. Hase, Perspective: chemical dynamics simulations of non-statistical reaction dynamics, *Philos. Trans. R. Soc., A*, 2017, **375**, 20160204.

30 M. J. Frisch, G. W. Trucks, H. B. Schlegel, G. E. Scuseria, M. A. Robb, J. R. Cheeseman, G. Scalmani, V. Barone, G. A. Petersson, H. Nakatsuji, X. Li, M. Caricato, A. V. Marenich, J. Bloino, B. G. Janesko, R. Gomperts, B. Mennucci, H. P. Hratchian, J. V. Ortiz, A. F. Izmaylov, J. L. Sonnenberg, D. Williams-Young, F. Ding, F. Lipparini, F. Egidi, J. Goings, B. Peng, A. Petrone, T. Henderson, D. Ranasinghe, V. G. Zakrzewski, J. Gao, N. Rega, G. Zheng, W. Liang, M. Hada, M. Ehara, K. Toyota, R. Fukuda, J. Hasegawa, M. Ishida, T. Nakajima, Y. Honda, O. Kitao, H. Nakai, T. Vreven, K. Throssell, J. A. Montgomery Jr, J. E. Peralta, F. Ogliaro, M. J. Bearpark, J. J. Heyd, E. N. Brothers, K. N. Kudin, V. N. Staroverov, T. A. Keith, R. Kobayashi, J. Normand, K. Raghavachari, A. P. Rendell, J. C. Burant, S. S. Iyengar, J. Tomasi, M. Cossi, J. M. Millam, M. Klene, C. Adamo, R. Cammi, J. W. Ochterski, R. L. Martin, K. Morokuma, O. Farkas, J. B. Foresman and D. J. Fox, *Gaussian 16, Revision C.01*, Gaussian, Inc., Wallingford CT, 2016.

31 Y. Zhao and D. G. Truhlar, The M06 Suite of Density Functionals for Main Group Thermochemistry, Thermochemical Kinetics, Noncovalent Interactions, Excited States, and Transition Elements: Two New Functionals and Systematic Testing of Four M06-class Functionals and 12 other Functionals, *Theor. Chem. Acc.*, 2008, **120**, 215–241.

32 K. Fukui, The Path of Chemical Reactions – The IRC Approach, *Acc. Chem. Res.*, 1981, **14**, 363–368.

33 D. G. Truhlar and B. C. Garrett, Variational Transition State Theory, *Annu. Rev. Phys. Chem.*, 1984, **35**, 159–189.

34 A. Fernandez-Ramos, B. A. Ellingson, B. C. Garrett and D. G. Truhlar, Variational Transition State Theory with Multidimensional Tunneling, *Reviews in Computational Chemistry*, ed. K. B. Lipkowitz and T. R. Cundari, Wiley-VCH, Hoboken, NJ, 2007, vol. 23, pp. 125–232.

35 J. Zheng, J. L. Bao, R. Meana-Pañeda, S. Zhang, B. J. Lynch, J. C. Corchado, Y.-Y. Chuang, P. L. Fast, W.-P. Hu, Y.-P. Liu, G. C. Lynch, K. A. Nguyen, C. F. Jackels, A. Fernandez Ramos, B. A. Ellingson, V. S. Melissas, J. Villà, I. Rossi, E. L. Coitiño, J. Pu, T. V. Albu, A. Ratkiewicz, R. Steckler, B. C. Garrett, A. D. Isaacson and D. G. Truhlar, *Polyrate 17-C*.

36 J. Zheng, J. L. Bao, S. Zhang, J. C. Corchado, R. Meana-Pañeda, Y.-Y. Chuang, E. L. Coitiño, B. A. Ellingson and D. G. Truhlar, *Gaussrate 2017-B*.

37 A. González-Lafont, J. Villà, J. M. Lluch, J. Bertrán, R. Steckler and D. G. Truhlar, Variational Transition State Theory and Tunneling Calculations with Reorientation of the Generalized Transition States for Methyl Cation Transfer, *J. Phys. Chem. A*, 1998, **102**, 3420–3428.

38 B. R. Ussing, C. Hang and D. A. Singleton, Dynamic Effects on the Periselectivity, Rate, Isotope Effects, and Mechanism of Cycloadditions of Ketenes with Cyclopentadiene, *J. Am. Chem. Soc.*, 2006, **128**, 7594.

39 Y. Oyola and D. A. Singleton, Dynamics and the Failure of Transition State Theory in Alkene Hydroboration, *J. Am. Chem. Soc.*, 2009, **131**(9), 3130–3131.

40 A. Patel, Z. Chen, Z. Yang, O. Gutiérrez, H. Liu, K. N. Houk and D. A. Singleton, Dynamically complex [6 + 4] and [4 + 2] cycloadditions in the biosynthesis of spinosyn A, *J. Am. Chem. Soc.*, 2016, **138**(11), 3631–3634.

41 S. R. Hare, A. Li and D. J. Tantillo, Post-transition state bifurcations induce dynamical detours in Pummerer-like reactions, *Chem. Sci.*, 2018, **9**, 8937–8945.

42 L. Verlet, Computer "Experiments" on Classical Fluids. I. Thermodynamical Properties of Lennard–Jones Molecules, *Phys. Rev.*, 1967, **159**, 98–103.

43 C. C. Levin, A Qualitative Molecular Orbital Picture of Electronegativity Effects on XH_3 Inversion Barriers, *J. Am. Chem. Soc.*, 1975, **97**(20), 5649–5655.

44 R. V. López, O. N. Faza and C. S. López, Dynamic Effects Responsible for High Selectivity in a [3,3] Sigmatropic Rearrangement Featuring a Bis-pericyclic Transition State, *J. Org. Chem.*, 2017, **82**(9), 4758–4765.

45 N. Mandal and A. Datta, Origin of Gold(i)-Catalyzed Intramolecular Diels–Alder Reaction: Evolution of Trappable Intermediates via Asynchronous Transition States, *J. Org. Chem.*, 2018, **83**(18), 11167–11177.

46 J. B. Thomas, J. R. Waas, M. Harmata and D. A. Singleton, Control Elements in Dynamically Determined Selectivity on Bifurcating Surface, *J. Am. Chem. Soc.*, 2008, **130**(44), 14544–14555.

47 S. Le and J. M. Goodman, Rapid Route-Finding for Bifurcating Organic Reactions, *J. Am. Chem. Soc.*, 2020, **142**(20), 9210–9219.

48 Y. Liu, S. Holm, J. Meisner, Y. Jia, Q. Wu, T. J. Woods, T. J. Martinez and J. S. Moore, Flyby reaction trajectories: Chemical dynamics under extrinsic force, *Science*, 2021, **373**(6551), 208–212.

49 N. Mandal and A. Datta, Dynamical Effects along the Bifurcation Pathway Control Semibullvalene Formation in Deazetization Reactions, *J. Phys. Chem. B*, 2018, **122**(3), 1239–1244.

50 A. H. Zewail, Femtochemistry: atomic-scale dynamics of the chemical bond, *J. Phys. Chem. A*, 2002, **104**(24), 5660–5694.

51 S. Pedersen, J. L. Herek and A. H. Zewail, The validity of the "diradical" hypothesis: direct femtosecond studies of the transition state structures, *Science*, 1994, **266**(5189), 1359.

52 D. V. Vidhani, M. E. Krafft and I. V. Alabugin, Gold(i)-Catalyzed Allenyl Cope Rearrangement: Evolution from Asynchronicity to Trappable Intermediates Assisted by Stereoelectronic Switching, *J. Am. Chem. Soc.*, 2016, **138**(8), 2769–2779.

53 C. Smuda, G. Gemmecker and T. Unruh, Quasielastic and inelastic neutron scattering study of methyl group rotation in solid and liquid pentafluoroanisole and pentafluorotoluene, *J. Chem. Phys.*, 2018, **128**(19), 194502.

54 S. Kozuch, Heavy atom tunneling in the automerization of pentalene and other antiaromatic systems, *RSC Adv.*, 2014, **4**, 21650–21656.

55 A. Nandi, A. Sucher and S. Kozuch, Ping-Pong Tunneling Reactions: Can Fluorine Jump at Absolute Zero?, *Chem.–Eur. J.*, 2018, **24**(61), 16348–16355.

56 S. Karmakar and A. Datta, Role of Heavy Atom Tunneling in Myers–Saito Cyclization of Cyclic Enyne-Cumulene Systems, *J. Phys. Chem. B*, 2016, **120**, 945–950.

57 NBO, F. Weinhold and C. R. Landis, *Valency and Bonding: A Natural Bond Orbital Donor–Acceptor Perspective*, Cambridge Univ. Press, Cambridge, 2005.

58 E. V. Anslyn and D. A. Dougherty, *Modern Physical Organic Chemistry*, University Science Books, Sausalito, CA, 2006.